Carbon 123 (2017) 26–33

Contents lists available at ScienceDirect

Carbon

journal homepage: www.elsevier.com/locate/carbon

Graphene and polytetrafluoroethylene synergistically improve the tribological properties and adhesion of nylon 66 coatings

Muhammad T. Masood [a], Evie L. Papadopoulou [a], José A. Heredia-Guerrero [a], Ilker S. Bayer [a], Athanassia Athanassiou [a], Luca Ceseracciu [b, *]

[a] Smart Materials, Istituto Italiano di Tecnologia, Via Morego 30, 16163, Genoa, Italy
[b] Materials Characterization Facility, Istituto Italiano di Tecnologia, Via Morego 30, 16163, Genoa, Italy

ARTICLE INFO

Article history:
Received 31 March 2017
Received in revised form
29 June 2017
Accepted 9 July 2017
Available online 12 July 2017

ABSTRACT

In this work, we exploit the bidimensional structure and high stiffness of graphene to improve the tribological response of nylon-based composites. Graphene nanoplatelets, coupled with polytetrafluoroethylene microparticles, synergistically improve the friction coefficient and wear rate, as well as the adhesion to the substrate. The enhancement, as high as threefold for both friction and wear rate at the optimal graphene concentration (0.5% in weight), depends upon the formation of a continuous, robust transfer film with the steel rubbing counterpart, as shown by Raman measurements. The graphene-nylon coating also shows three-fold improved adhesion to the underlying substrate, attributed to the high surface energy of graphene.

1. Introduction

The use of polymers and polymer nanocomposites is increasingly growing in a number of tribology related components, such as bearings, gears, seals, vacuum pumps as well as components for prosthesis and implants in biological or medical applications, to name a few [1,2]. Their increased usage is observed particularly in areas where traditional fluid lubricants cannot be used, or the formation of hard debris must be avoided [3]. Good resistance to sliding contact, together with strong adhesion to the underlying substrate, are also desirable when surface coverage is involved, with coatings as paints and varnishes [4], in microelectronic systems [5] or machine parts [6], etc. Polymeric coatings are a class of the family of solid lubricants, alternative to the spraying of solvent-suspended particles [7–9] when the application of the latter is hindered by incompatible substrate, unadapt environment, danger of contamination. Indeed, the elimination of harmful solvents is one of the objectives of Green Tribology, a growing field within the broader one of Green Chemistry, dedicated specifically to reduce the environmental impact of tribological systems [10,11].

Aliphatic polyamides are extensively used as sliding parts in food packaging, automobile parts, engineering products and bearings [12–14]. Among various polyamides, nylon 66 has been widely used in industry due to its excellent physico-chemical properties, such as high melting point, low permeability, low melting viscosity, ductility, heat resistance, etc. [15]. However, despite the good mechanical and tribological properties of polyamides as bulk components [16], their use as coatings is limited by their poor adhesion to substrates, due to their low surface energy and weak mechanical interlocking mechanism [17]. A possible approach to the improvement of adhesion is based on the addition of different fillers, exploiting their stronger interaction with the substrate or the improved formation of anchor points for mechanical interlocking [18,19]. Yet the main purpose of fillers is to improve the mechanical properties of polymeric materials, and, among them, their tribological response. The most common fillers to reduce friction and wear include hard ceramics such as alumina, polytetrafluoroethylene (PTFE), molybdenum-disulfide (MoS_2) and carbon based materials, often prepared in nanometric size [20,21]. However, these fillers have some limitations, for instance PTFE is well-known for low friction, but has poor wear resistance [22], MoS_2 performs poorly in the presence of humidity [23,24] and graphite has restriction of operating in dry or vacuum environment [25]. Compared to such conventional fillers, graphene has gained great attention in recent years because of its exceptional electrical [26], mechanical, thermal, structural properties and has already shown promising results in tribology as a lubricant additive [27]. As an additive, graphene can have a strong effect on the mechanical

* Corresponding author.
E-mail address: luca.ceseracciu@iit.it (L. Ceseracciu).

http://dx.doi.org/10.1016/j.carbon.2017.07.026

properties of a composite material, owing to its high strength (~130 GPa) and elastic modulus (0.5–1 TPa) [28,29]. Graphene has been employed as a filler for different polymers, among which Lahiri et al. incorporated graphene nanoplatelets (GNPs) as a reinforcement element in ultrahigh molecular weight polyethylene to improve its fracture toughness and tensile strength [30], Xu et al. reported the enhancement of tensile strength and Young's modulus by the in situ polymerization of graphene nylon 6 polymer [31], Cataldi et al. studied the improvement in modulus of stiff and soft polymers by the addition of graphene with different thermal treatments [32]. Apart from effect on bulk properties of a composite material, graphene has unique characteristics of interfacial interaction with different substrates, such as silica, copper and nickel [33,34].

Despite the physical properties that make graphene a promising candidate as a solid lubricant or as an additive, such as its bidimensional structure, high strength and low permeability to gases [35], its use in the field of tribology is relatively unexplored, if compared to other carbon-based materials [36]. Graphene nanoplatelets have been proposed as a thin solid lubricant [37,38] and have shown high wear resistance especially at nanoscale [39,40], but only in few works its performance in macroscopic solid materials has been investigated [41,42]. Notably, Kandanur et al. reduced the wear rate of PTFE by addition of 10 wt% graphene platelets [43]. A limiting factor to the widespread use of graphene as a tribological material is its friction coefficient (0.1–0.2) [44] which is still higher than that of the best performing materials, such as PTFE (<0.05).

In this work, we aim to study polymer composites, containing GNPs as solid lubricants. Nylon 66 is chosen as the polymer matrix, due to its wide use in the industry. Nylon 66 is usually processed by extrusion or hydraulic press to form bulk specimens, or dissolved in solvents like formic and hydrochloric acids or cresol [45,46] resulting in porous membrane with poor mechanical properties, unsuitable for use where tough mechanical parts are needed. Recently, a new solution-based method was developed [47] to produce non-porous films with good mechanical properties, which were further improved by the addition of GNPs. Here, we propose this novel route for the study of nylon 66/GNPs as a coating incorporating also PTFE for tribology application. The GNPs/nylon 66/PTFE composites show strong adhesion and a three-fold reduction in friction and wear rate, compared to the pure nylon 66. The best performance was obtained for an amount of GNPs of 0.5% in weight.

2. Materials and methods

Nylon 66 (PA66) was purchased from Sigma-Aldrich (molecular weight MW = 120,000; degree of polymerization DP = 531; density $\rho = 1.14$ g/mL). Grade Pure G+ Graphene nanoplatelets (GNPs), with lateral dimension of a few micrometres and a thickness of a few nanometers [48], were kindly provided by Directa Plus (Lomazzo (CO) – Italy). Polytetrafluoroethylene (PTFE) with nominal particle size of 1 μm, aluminum oxide nanoparticles with nominal particle size of 13 nm and Ethyl Cyanoacrylate (Permabond 105) were purchased from Sigma-Aldrich.

Reagent grade solvent trifluoroacetic acid (TFA), dimethyl sulfoxide (DMSO) and acetone were purchased from Sigma-Aldrich and used as received.

2.1. Sample preparation

Composite coatings of nylon 66 were prepared using different GNPs concentrations while keeping constant the concentration of PTFE with respect to the nylon 66. The preparation of the nylon 66 is described in detail in Ref. [47]. Briefly, nylon 66 was first dissolved in solution of TFA and acetone with 1:1 vol ratio to obtain 7 wt% polymer in solution. After the nylon 66 pellets were completely dissolved, PTFE was added to the solution at concentration ratio of 5 wt% with respect to nylon 66. GNPs were then added at different weight fractions, ranging from 0 wt% to 3 wt% with respect to nylon 66. Solutions were bath sonicated at 40 Hz for 3 h and at 59 Hz after 24 h to get homogeneous dispersion of both PTFE particles and GNPs. The choice to include PTFE in all composites was taken after screening tests (not reported) showed significantly higher friction when it was not added.

Glass substrates were cut to a rectangular shape, cleaned with acetone and bath sonicated for 60 min for the removal of residues. A simple dip coating method was used for the deposition: the substrates were dipped in the solution for 10–15 s and left in fume hood for the solvent to evaporate. All the samples prepared and their labels are presented in Table 1.

Additional samples were fabricated with the same technique substituting GNPs with alumina nanoparticles, as a reference for the tribological tests. Details on these samples are reported in the supporting information, Table S1. Samples of Ethyl Cyanoacrylate (ECA) were also deposited with the same technique starting from a solution of dimethyl sulfoxide (DMSO) and acetone, as a reference for the adhesion tests.

2.2. Morphological characterization

The morphology of the films was studied by Optical Microscopy (Leica DM 2500 M) and Scanning Electron Microscopy (SEM, JEOL JSM-6490AL operating at 10 kV and JEOL JSM 7500FA operating at 5 kV). Films were sputtered with a thin layer of gold or graphite before observation to improve conductivity.

Grazing Incidence X-ray Diffraction (GIXRD) analysis was performed on a Rigaku Smartlab equipped with a 9 kW CuKα rotating anode, operating at 40 kV and 150 mA. A Göbel mirror was used to convert the divergent X-ray beam into a parallel beam and to suppress the Cu Kβ radiation, while a 0.5° Parallel Slit Analyzer was employed in the receiving optics. The diffraction patterns were collected with a fixed grazing incidence angle ω of 3° and over a 2θ angular range from 7° to 60°, with a step size of 0.05°. The specimens were placed on a zero-diffraction quartz substrate and measured at room temperature. GIXRD data analysis was carried out with the PDXL 2.1 software from Rigaku.

2.3. Mechanical characterization

The Young's modulus and hardness of the samples were characterized by nanoindentation on an Anton Paar UNHT equipped with a diamond Berkovich tip. Maximum load was 1 mN, loading and unloading time 30 s, with a dwell time at maximum load of 30 s to allow viscous relaxation. Young's modulus E and hardness H

Table 1
Labels and PTFE and GNPs concentration of the prepared samples.

Sample label	Concentration (Nylon 66 to 100%)	
	PTFE wt.%	GNPs wt.%
P0G0	0	0
P5G0	5	0
P5G0.1	5	0.1
P5G0.2	5	0.2
P5G0.3	5	0.3
P5G0.4	5	0.4
P5G0.5	5	0.5
P5G1	5	1.0
P5G2	5	2.0
P5G3	5	3.0

were calculated from the unloading curves with the Oliver & Pharr method. At least 10 repetitions were conducted for each material, and results are presented as average value and standard deviation.

2.4. Tribological characterization

Multi-pass scratch tests were performed on a Micro-combi tester (Anton Paar Gmbh, Germany), to evaluate friction and wear resistance. A bearing steel ball of 500 μm radius was used as a counterpart for rubbing. The tip displacement rate was 10 mm/min for a reciprocating distance of 4 mm, corresponding to a frequency f = 0.042 Hz, under the constant load of 1 N, corresponding to a Hertzian pressure $p \sim 90\,MPa$, for 75 cycles, corresponding to 30 min. All the friction and wear tests were carried out at laboratory conditions (21 ± 1 °C, 50 ± 5%RH).

The average values of steady coefficient of friction, following the running-in phase, were extracted from the experimental data plots of friction coefficient. A typical friction trace is reported in the supporting information, Fig. S2. All the data here are the average of five replicate measurements for each material. The evolution of friction as a function of the number of cycles is also reported in the supporting information (Fig. S3).

After each test, the depth of the wear scar d was measured using a stylus surface profiler (DektakXT, Bruker). Each scar was measured 5 times and the average was calculated. The wear volume, ΔV, of the specimen was calculated from geometrical considerations, with Equation (1):

$$\Delta V = \frac{L}{2}\, r^2 \left(\cos^{-1}\left(\frac{r-d}{r}\right) - \frac{\sqrt{r^2-d^2}}{r} \right) \quad (1)$$

where L is the length of the stroke in one cycle and r is the radius of the counterpart steel ball. The wear rate was calculated by the ASTM G-99 standard wear rate formula:

$$K = \frac{\Delta V}{F \times N \times L} \quad (2)$$

where F is the applied load (N), L the stroke length in one cycle (m) and N represents the total number of cycles, so that NL is the total sliding length [49].

Moreover, the adhesion of coatings deposited on the glass substrates was evaluated by a progressive scratch test, during which the load was increased linearly from 0.03 N (Hertzian pressure $p \sim 60\,MPa$) to 10 N ($p \sim 190\,MPa$) over a scratch length of 2 mm, with a sliding rate of 1 mm/min and acquisition rate of 30 Hz. After each test, optical images were acquired to examine the damage mechanisms and to evaluate the failure critical load, corresponding to the load at which the glass substrate is exposed. In order to evaluate the significance of the measured values, additional tests were performed on Ethyl Cyanoacrylate (ECA). Such polymer is specifically designed as an instant adhesive, it was therefore taken as a positive control.

2.5. Chemical characterization

μRaman spectra were collected at ambient conditions using a Horiba Jobin Yvon LabRAM HR800 spectrometer, equipped with a microscope. A 632.8 nm excitation line, in backscattering geometry through a 50 × objective lens, was used to excite the specimens, at the low power of ~0.25 mW. The experimental set-up consists of a grating 600 lines/mm with spectral resolution of approximately 1 cm^{-1}. Raman spectra were collected from the pristine surface, as well as from the scratch, after the wear test and from the steel ball used as rubbing counterpart.

3. Results and discussion

3.1. Films morphology and structure

Uniform composite films were obtained through the dipping method, with thickness varying among samples between 10 and 20 μm. Roughness of the films was measured on a stylus optical profiler (DektakXT, Bruker), yielding values in the range of 765–780 nm. Fig. 1a–d shows the optical images of the surface of selected samples. The nylon 66 matrix appears dense and non-porous. GNPs are clearly visible in loaded samples, owing in part to the transparency of nylon 66 to visible light. GNPs distribution is fairly homogeneous in all samples, with tendency towards slightly larger clusters as the GNPs concentration is increased. These observations were confirmed by SEM images on selected samples, reported in Fig. 2a–b: as the amount of GNPs is increased, platelets tend to form slightly larger clusters. PTFE particles can also be seen in both samples.

X-ray diffraction spectra were acquired on selected samples and are shown in Fig. 2c. The main peaks are ascribed to the triclinic α phase of nylon 66, at 20°, corresponding to the (100) plane, and at 24°, corresponding to the (010)/(110) doublet. Morphology-wise, the former is associated with the intra-sheet, the latter to inter-sheet diffraction. A broad amorphous halo is also evident, centered at around 22° [50]. Considering the intensities of the crystalline peaks and the amorphous halo, no appreciable differences in the crystallinity are evident. On the other hand, the ratio between the (100) and the (010)/(110) peaks, shown in Fig. 2d, is slightly modified for GNPs concentration larger than 0.5%, going from 0.76 (P5G0 and P5G0.5 samples) to 0.52 (P5G1) and to 0.48 (P5G3). Such phenomenon was observed already, and is associated to the GNPs intervening in the crystallization from solution, with the effect of weakening the intrasheet bonding between crystalline sheets [47]. Interestingly, the addition of a small amount of graphene, up to 0.5 wt%, does not modify the ratio, suggesting that the platelets thickness is low enough to not affect the structure, i.e. dispersion is good and aggregation minimal.

3.2. Mechanical and tribological properties

Nanoindentation results are shown in Fig. 3a. Young's modulus is weakly affected by variations in GNPs concentration. The only value significantly higher than the rest is that of P5G0.5 samples ($p < 0.01$ as calculated through ANOVA). Such increment is in line with our previous findings in a similar system [32] and suggests good dispersion of the fillers as compared to the other compositions. Interestingly, hardness increases only slightly and with little statistical significance as the GNPs concentration is augmented. Overall, the mechanical properties can be considered weakly affected by the composition, therefore any variation observed in the tribological response can not be explained only as a consequence of such properties.

The friction coefficient and wear rate of the materials as a function of GNPs concentration are presented in Fig. 3b and c, respectively. It can be observed that the pure PA66 film has a coefficient of friction of ca. 0.19, whereas addition of PTFE fillers results in a significant reduction of the friction coefficient to ca. 0.12. The addition of GNPs results in a further decrease of the coefficient of friction: increasing the GNPs concentration from 0.1% to 0.5% results in a large decrease in coefficient of friction, with the lowest value, 0.06, obtained for the P5G0.5 samples. As the GNPs concentration increases further, from 1.0% to 3.0%, the beneficial effect of the GNPs is reduced, and the values of the friction coefficient increase up to ca. 0.13. The specific effect of GNPs in combination with PTFE can be better appreciated if compared with similar

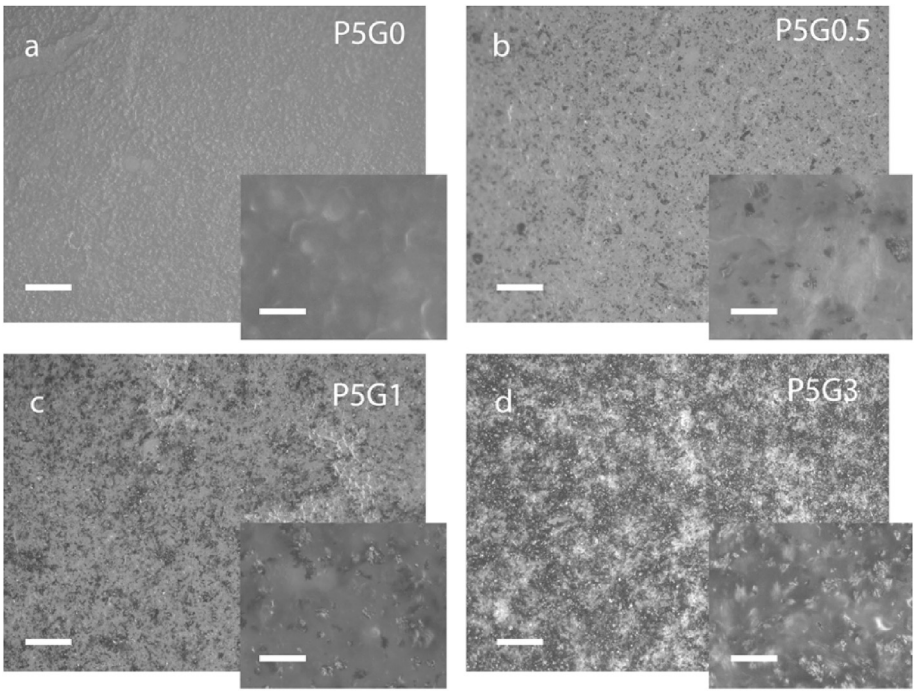

Fig. 1. Optical images of the studied nanocomposites: a) P5G0, b) P5G0.5, c) P5G1, d) P5G3. Higher magnification is shown for each material in the inset. Scale bars are 50 μm in the main images, 10 μm in the insets.

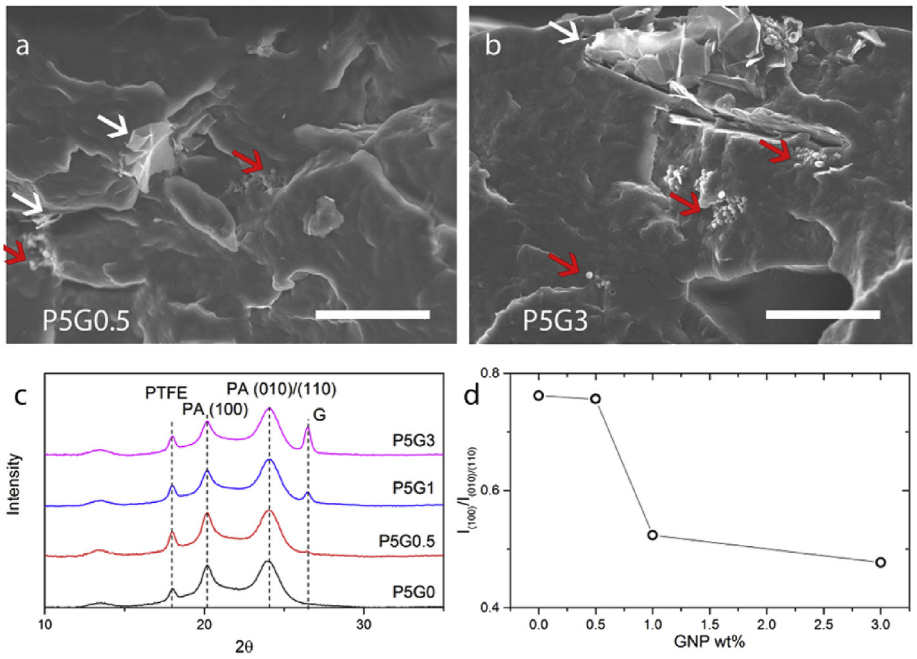

Fig. 2. SEM cross-sections of selected samples, scale bars 50 μm: a) P5G0.5 and b) P5G3; GNPs are indicated by white arrows, PTFE microparticles by red arrows. A relatively large GNPs cluster is visible at the surface of P5G3; c) GIXRD spectra on P5G0, P5G0.5, P5G1 and P5G3 samples; d) evolution of the $I_{(100)}/I_{(010)/(110)}$ peaks ratio as a function of graphene content. (A colour version of this figure can be viewed online.)

composite coatings in which graphene is replaced with another effective low-friction additive, such as aluminium oxide. Direct comparison, reported in Fig. S1 of the Supporting information, shows values of friction in the same order, but not as low as our best results, obtained with GNPs.

A similar behavior can be seen in the wear rate measurements: the increment of the GNPs concentration improves the wear resistance, which exhibits a minimum at 0.5% GNPs concentration. As shown in Fig. 3c, the wear rate drops from 16.21×10^{-4} mm^3/Nm for the P5G0 sample, down to 5.98×10^{-4} mm^3/Nm for the P5G0.5 sample. Similar to the friction coefficient case, our results compare favourably to those obtained on materials reinforced with aluminium oxide (Fig. S1 in the supporting information). It is worth noting that it was not possible to measure wear rate of the pure

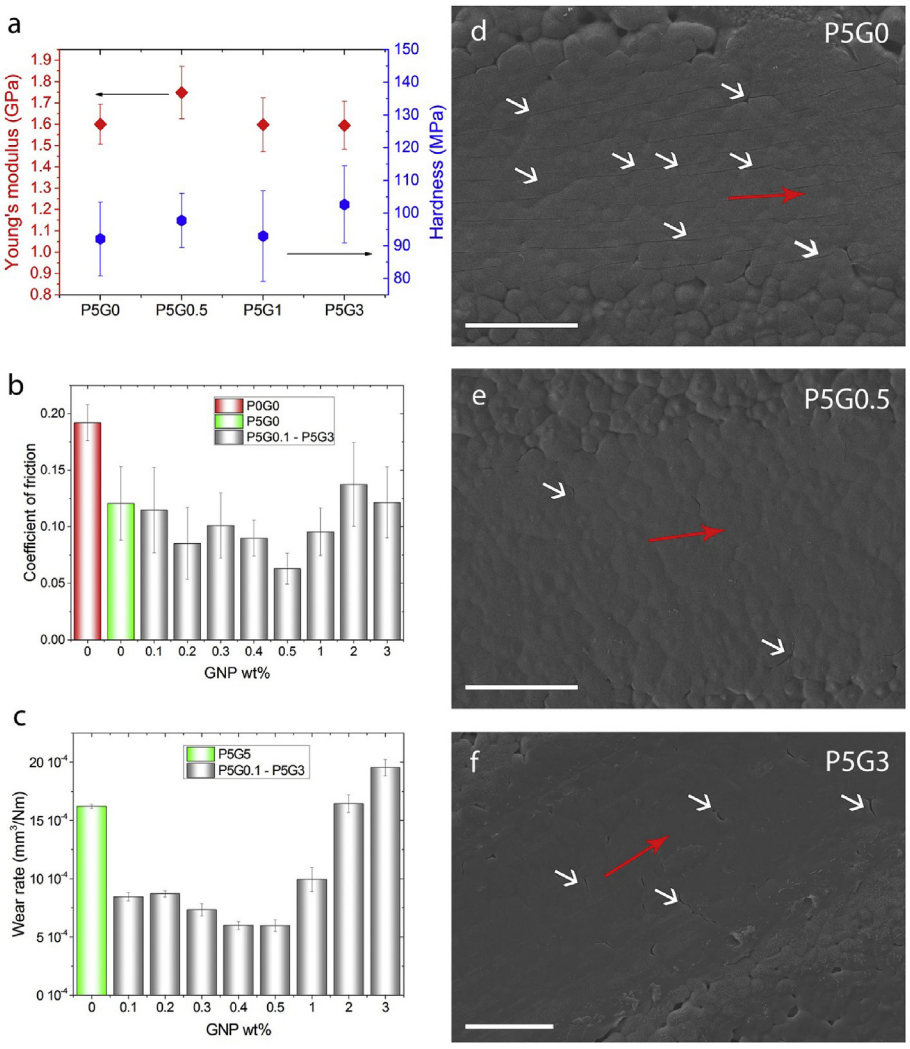

Fig. 3. (a) Mechanical properties, (b) coefficient of friction and (c) wear rate of nylon/PTFE composite at different GNPs concentrations (d–f) SEM images scratched surfaces from selected samples, scale bars are 50 μm, red arrows indicate the testing direction: in P5G0 (d) arrows indicate longitudinal cracks; in P5G0.5 (e) only a few transverse cracks are visible, whereas in P5G3 (f) they are more frequent. (A colour version of this figure can be viewed online.)

nylon film due to its poor adhesion with the glass substrate. It was however possible to obtain reliable values of the friction coefficient, which is a less stressful test for the material, only by attaching the films to the substrate with thin double side tape.

Fig. 3d–f show the SEM images of the scratched surface of the P5G0, P5G0.5 and P5G3 samples. All present fairly smooth surfaces, which suggests that the wear mechanism is the adiabatic formation of a transfer film, typical for semi-crystalline polymers [51]. Only the P5G3 sample presents few debris at the sliding path edges. P5G0, on the other hand, exhibits numerous longitudinal cracks (Fig. 3d), probably due to plastic deformation which nucleates below the contact area [52] and, when the stress imposed by the steel ball is released, maintains the deformation, so that a tensile stress is generated on the layer of material above, deformed elastically, leading to fracture. In the presence of GNPs, damage has the form of transverse, rather than longitudinal, cracks, with just a few occurrences in the P5G0.5 samples (Fig. 3e) and a larger number in the P5G3 samples (Fig. 3f). Transverse cracks are attributed to decohesion at the Nylon 66/GNPs interface, which is typical in composites based on layered nanofillers [53] and leads to the formation of debris in the case of P5G3 samples.

The improvement can be attributed to the formation of a transfer film between the coating and the rubbing counterpart: a thin layer of material is transferred to the steel ball, and spread along the scratching area, so the low-friction material is present in both sliding surfaces. PTFE is, indeed, well known for creating a transfer film upon sliding contacts, which reduces substantially the friction of material [54]. On the other hand, the presence of a transfer film by itself does not guarantee low wear rate as well: PTFE, with its poor performance when used as a bulk material, well exemplifies this counterintuitive behavior, while the addition of fillers, especially alumina, improves this aspect by several orders of magnitude [54–57]. In PTFE, fillers bear part of the load and arrest crack propagation and hinder large-scale fragmentation, so that material removal is lower, and in some cases induce chemical bonding of the formed film to the sliding surfaces [55].

In order to highlight the mechanisms of formation of transfer films and possible chemical interactions, Raman studies were performed on the pristine surface of the samples, as well as on the scratch formed on the surface after the wear test. In Fig. 4a the Raman spectra of the P5G0 and P5G0.5 films are shown. The spectra taken from the pristine surface are those typical of the nylon 66 spectra prepared with the TFA-acetone solvent [47]. Briefly, the peak at 1636 cm^{-1} is assigned to the amide I group, while the peak at 1296 cm^{-1} is assigned to CH_2 twisting mode, the peak at 1445 cm^{-1} and the band centered at approximately 2908 cm^{-1} are assigned to

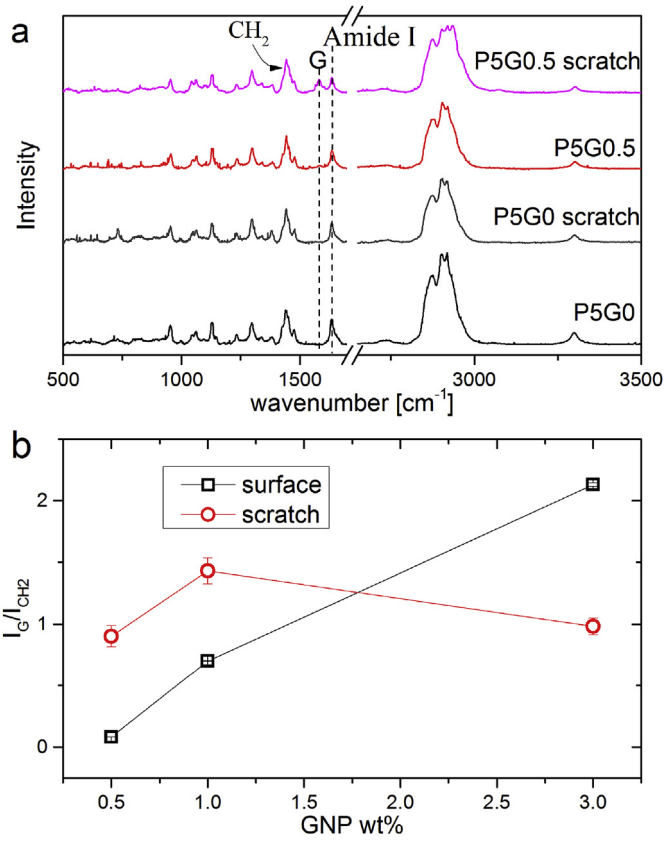

Fig. 4. a) Raman spectra of P5G0 and P5G0.5 samples, on pristine and scratched surfaces; b) I_G/I_{CH3} peaks ratio as a function of graphene concentration, on pristine and scratched surfaces. (A colour version of this figure can be viewed online.)

CH_2 bending and stretching modes, respectively. Finally, the N–H stretching of the amide A is observed at 3300 cm^{-1}. In the same figure, the Raman spectra of the nylon 66/graphene samples is depicted for the 0.5% graphene concentration, where the G peak of graphene is located at 1580 cm^{-1}. Increasing the graphene concentration results in a higher intensity of G peak and the appearance of the other characteristic peaks of graphene, such as the D peak (~1345 cm^{-1}) and the 2D peak (~2700 cm^{-1}) (spectra not shown here). The intensities of the G peak, normalized by the intensity of methylene twisting peak at 1445 cm^{-1}, are shown for the pristine surface and the scratch in Fig. 4b. As expected, the normalized G peak increases with increasing graphene concentration for the pristine surface. Considering the spectrum acquired on the steel counterpart (Fig. S4 in the supporting information), the formation of a transfer film is confirmed by the presence of graphene.

From the spectra acquired on the scratched lines, Fig. 4b, no chemical interactions of GNPs with either PTFE or the nylon 66 matrix are visible; we attribute to the high surface energy of GNPs the improvement of the physical adhesion to both surfaces, while their bidimensional structure facilitates plains sliding, much like the effect of well-disperse modified nanoclay added to nylon 6 [53]. On the other hand, the variation of the G peak as a function of GNPs concentration suggests that the formation of a graphene transfer film does not follow the same behavior in all composites: the amount of graphene on the scratch imprint is higher than that on the untested surface in the case of low graphene concentration, up to 0.5 wt %, and is lower for concentration of 1.0 wt % and above, as shown in Fig. 4b. In the former case GNPs are exposed during the first sliding cycles until a robust film is formed. In the latter case, instead, we attribute the lower amount of GNPs to low distance in between neighboring GNPs, so that the elastic mismatch with the matrix leads to mechanical removal of small platelet clusters which can induce third-body abrasion on the soft polymer, as shown by Khedkar et al. [56]. A similar influence of the platelets size, in a broader range of size, can be seen comparing graphene and graphite as fillers: the difference in wear rate can be as high as an order of magnitude, for a given concentration [43]. The fact that the Young's modulus is not increased with the GNPs content confirms, indeed, that the dispersion is not optimal beyond a threshold value. A scheme of this mechanism for the formation of transfer film and its dependency on the amount of GNPs is shown in Fig. 5.

This mechanism is compatible with the observations of the scratched areas (Fig. 3d–f): in the absence of graphene the visible longitudinal cracks indicate plastic deformation below the surface, similar to ductile plowing. The addition of graphene by reducing the friction hinders the tip penetration, so that overall damage is lower and consists only of few cracks, in locations probably weaker from the production process.

The role of PTFE in enhancing the tribological response of the

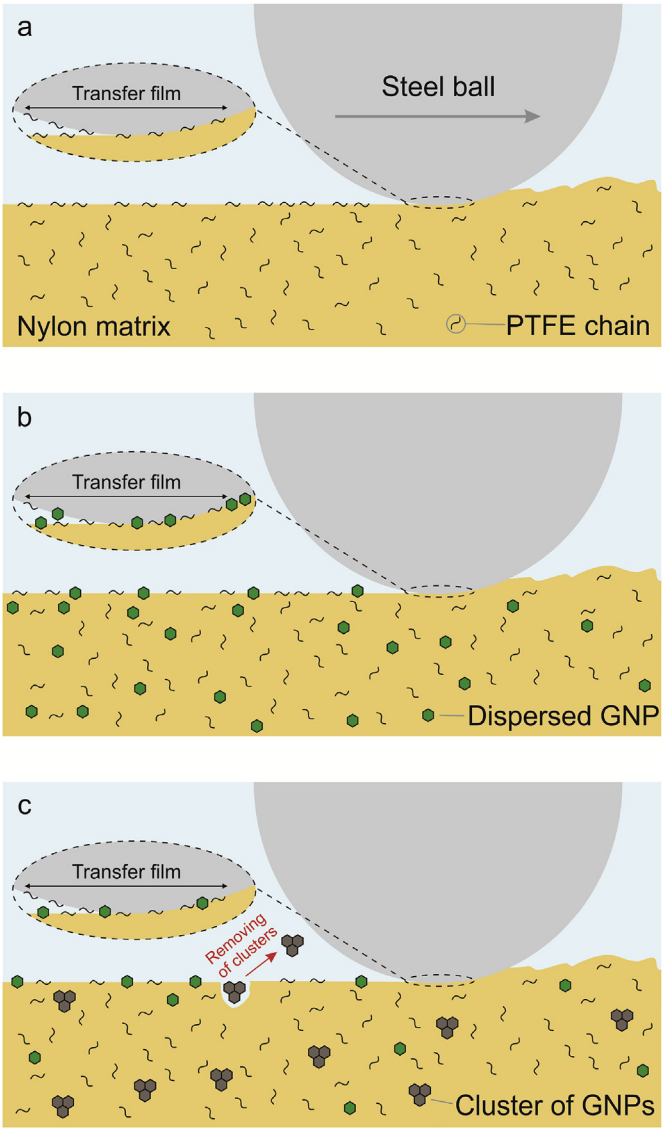

Fig. 5. Proposed mechanism of transfer film formation for different GNPs loading: in (a) in the absence of GNPs, PTFE forms a transfer film with low friction but poor wear resistance; (b) with the addition of 0.3–0.5 wt % GNPs, the transfer film is continuous and reduces dramatically the wear rate; (c) larger amounts of GNPs induce the formation of clusters, which are removed by the sliding ball, hindering the formation of an effective transfer film. (A colour version of this figure can be viewed online.)

material is quantitatively more difficult to define, as its presence was not detectable by Raman spectroscopy. Phenomenologically, its presence together with graphene reduces the friction coefficient to lower values than those of composites with the same amount of GNPs but without PTFE. It is thought, therefore, that the presence of GNPs has the dual effect of participating in the formation of the low-friction transfer film and of reinforcing the PTFE, thus reducing the wear rate, due to its rigidity and strength.

Overall, this mechanism is supported by the running-in evolution of friction coefficient, reported in Fig. S3: in the absence of graphene (sample P5G0), after a few cycles at low friction (≈ 0.09) a progressive increment indicates the removal of the transfer film; for low amounts of graphene (P5G0.5 and P5G1) friction decreases rapidly and remains stable, whereas for higher amount (P5G3), friction does not show a reduction as large.

3.3. Adhesion

To evaluate the adhesion between the composite films and the glass substrate, progressive scratch tests were performed on films deposited on glass slides. The critical load for failure was then optically defined using the built-in microscope and the results are presented in Fig. 6a. The choice of glass as a substrate was dictated by the experimental need to univocally identify the onset of damage, which would be unreliable on metallic materials. Although extrapolation of our results would be speculative, the improvement granted by GNPs can be evaluated considering its intrinsic adhesion force: few-layers graphene has been shown both experimentally [58] and theoretically [33] that its adhesion to silica and copper is similar, which suggests that the adhesion improvement from graphene as a filler might be generalized. As expected, the pure nylon 66 films (P0G0 samples) did not adhere on the glass substrate due to the low surface energy of both materials. Similarly, the P5G0 sample showed very low adhesion, with visible damage starting at 3 N. Addition of GNPs, on the other hand, increased the adhesion gradually, with maximum values for the P5G0.3, P5G0.4, P5G0.5 samples. Further addition of graphene is detrimental for adhesion, although the values of critical load are still higher than those of the samples without GNPs.

In order to overcome the limitations of the testing technique to provide absolute values of adhesion, and thus estimate the significance of our materials, we conducted tests on a material specifically designed as a bonding agent, ethyl cyanoacrylate. The critical load in this case was indeed higher, as expected, but only by a factor of 2 over our best-performing materials. We consider this comparison an indirect confirmation of the effectiveness of GNPs to facilitate the application of nylon 66 as a robust coating.

Observation of the damaged samples using the built-in optical microscope indicates two damage mechanisms, namely delamination and shear-driven material removal. The former is visible in the absence of graphene and is characterized by uplift of an area around the scratch mark (red arrow in Fig. 6b). The latter can be identified by the removal of the film and the exposure of the glass substrate and appears at low load, ca. 3 N, in the P5G0 samples, while it was not measurable in the unfilled polymer, as mentioned above. With the addition of GNPs, the critical load increases fairly linearly, reaching the maximum for the P5G0.5 sample, which in most cases did not show either damage mechanism (Fig. 6d). For higher GNPs concentration, values are slightly progressively lower.

Overall, the improvement follows the same trend as the wear tests, with the best performance from the P5G0.5 sample. The enhancement provided by graphene is attributed to its high interfacial energy. At higher GNPs concentration, similarly to the tribological results, the formation of small clusters of GNPs induces the formation of defects at interface, causing the earlier onset of film detachment.

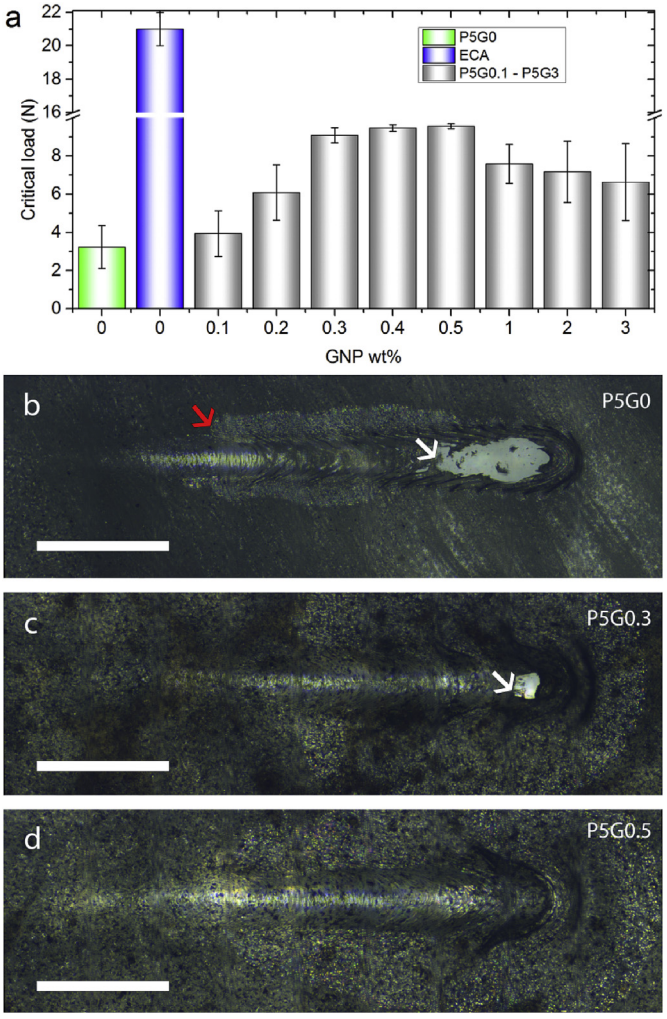

Fig. 6. (a) Progressive scratch test critical load of nylon 66/PTFE/GNP composites and ECA as reference; Optical images of P5G0 (b), P5G0.3 (c) and P5G0.5 (d). Scale bar is 500 μm. In the absence of graphene (panel b) two damage mechanisms are present: delamination (red arrow) and substrate decohesion (white arrow). With the addition of GNPs, both mechanisms are hindered, first delamination (panel c), then substrate decohesion (panel d). (A colour version of this figure can be viewed online.)

4. Conclusions

We have developed a composite coating based on solvent-cast nylon 66 with the addition of PTFE and graphene nanoplatelets in several concentrations. We have found that the friction coefficient, wear rate and adhesion to the glass substrate are greatly improved by the addition of both fillers, provided that the graphene nanoplatelets achieve good dispersion and do not modify the intercrystallites structure of nylon 66. If this condition is fulfilled, graphene creates a robust transfer film that optimizes the tribological response and increases the interfacial energy. Such optimal condition was found at 0.5 wt% GNPs, whereas further addition of graphene leads to flakes agglomerates easy to remove upon scratching.

Acknowledgements

We would like to acknowledge Mr. Sergio Marras for help in GIXRD measurements and Mrs. Alice Scarpellini and Mr. Simone

Lauciello for SEM imaging. We also acknowledge Directa Plus for kindly providing the graphene nanoplatelets.

Appendix A. Supplementary data

Supplementary data related to this article can be found at http://dx.doi.org/10.1016/j.carbon.2017.07.026.

References

[1] B.J. Briscoe, S.K. Sinha, Tribological applications of polymers and their composites: past, present and future prospects, Tribol. Inter Eng. 55 (2008) 1–14.
[2] J. Villanueva, L. Trino, J. Thomas, D. Bijukumar, D. Royhman, M.M. Stack, M.T. Mathew, Corrosion, tribology, and tribocorrosion research in biomedical implants: progressive trend in the published literature, J. Bio. Tribo. Corros. 3 (1) (2016) 1.
[3] D.L. Burris, B. Boesl, G.R. Bourne, W.G. Sawyer, Polymeric nanocomposites for tribological applications, Macromol. Mater Eng. 292 (4) (2007) 387–402.
[4] D.J. Mihora, A.C. Ramamurthy, Friction induced damage: preliminary numerical analysis of stresses within painted automotive plastics induced by large curvature counterfaces, Wear 203 (1997) 362–374.
[5] Y.C. Jung, B. Bhushan, Contact angle, adhesion and friction properties of micro- and nanopatterned polymers for superhydrophobicity, Nanotechnology 17 (19) (2006) 4970–4980.
[6] J.I. Nozawa, T. Komoto, T. Kawai, H. Kumehara, Tribological properties of polymer-sheet-adhered metal hybrid gear, Wear 266 (9–10) (2009) 893–897.
[7] C. Donnet, A. Erdemir, Historical developments and new trends in tribological and solid lubricant coatings, Surf. Coat. Tech. 180 (2004) 76–84.
[8] G. Zhang, H. Liao, H. Li, C. Mateus, J.M. Bordes, C. Coddet, On dry sliding friction and wear behaviour of PEEK and PEEK/SiC-composite coatings, Wear 260 (6) (2006) 594–600.
[9] M. Arita, Y. Yasuda, K. Kishi, N. Ohmae, Investigations of tribological characteristics of solid lubricants exposed to atomic oxygen, Tribol. T 35 (2) (1992) 374–380.
[10] M. Nosonovsky, B. Bhushan, Green tribology: principles, research areas and challenges INTRODUCTION, Philos. T R. Soc. A 368 (1929) (2010) 4677–4694.
[11] B.P. Chang, H. Md Akil, M.H. Zamri, Tribological characteristics of green biocomposites, in: M. Jawaid, S.M. Sapuan, O.Y. Alothman (Eds.), Green Biocomposites: Manufacturing and Properties, Springer International Publishing, Cham, 2017, pp. 149–179.
[12] V. Siracusa, P. Rocculi, S. Romani, M. Dalla Rosa, Biodegradable polymers for food packaging: a review, Trends Food Sci. Technol. 19 (12) (2008) 634–643.
[13] C.M. Sonsino, E. Moosbrugger, Fatigue design of highly loaded short-glass-fibre reinforced polyamide parts in engine compartments, Int. J. Fatigue 30 (7) (2008) 1279–1288.
[14] M.T. Demirci, H. Duzcukoglu, Wear behaviors of Polytetrafluoroethylene and glass fiber reinforced Polyamide 66 journal bearings, Mater Des. 57 (2014) 560–567.
[15] J.H. Lee, S.G. Lee, K.Y. Choi, J.J. Liu, Crystallization and melting behavior of nylon 66 poly(ether imide) blends, Polym. J. 30 (7) (1998) 531–537.
[16] S. Apichartpattanasiri, J.N. Hay, S.N. Kukureka, A study of the tribological behaviour of polyamide 66 with varying injection-moulding parameters, Wear 251 (2001) 1557–1566.
[17] K.T. Wan, A. DiPrima, L. Ye, Y.W. Mai, Adhesion of nylon-6 on surface treated aluminium substrates, J. Mater Sci. 31 (8) (1996) 2109–2116.
[18] S.A. Meguid, Y. Sun, On the tensile and shear strength of nano-reinforced composite interfaces, Mater Des. 25 (4) (2004) 289–296.
[19] A. Dorigato, A. Pegoretti, The role of alumina nanoparticles in epoxy adhesives, J. Nanoparticle. Res. 13 (6) (2011) 2429–2441.
[20] V.N. Aderikha, V.A. Shapovalov, Effect of filler surface properties on structure, mechanical and tribological behavior of PTFE-carbon black composites, Wear 268 (11–12) (2010) 1455–1464.
[21] Y. Xue, W. Wu, O. Jacobs, B. Schadel, Tribological behaviour of UHMWPE/HDPE blends reinforced with multi-wall carbon nanotubes, Polym. Test. 25 (2) (2006) 221–229.
[22] W.G. Sawyer, K.D. Freudenberg, P. Bhimaraj, L.S. Schadler, A study on the friction and wear behavior of PTFE filled with alumina nanoparticles, Wear 254 (5–6) (2003) 573–580.
[23] H.S. Khare, D.L. Burris, The effects of environmental water and oxygen on the temperature-dependent friction of sputtered molybdenum disulfide, Tribol. Lett. 52 (3) (2013) 485–493.
[24] J.K. Lancaster, A review of the influence of environmental humidity and water on friction, lubrication and wear, Tribol. Int. 23 (6) (1990) 371–389.
[25] N. Kumar, S. Dash, A.K. Tyagi, B. Raj, Super low to high friction of turbostratic graphite under various atmospheric test conditions, Tribol. Int. 44 (12) (2011) 1969–1978.
[26] P. Cataldi, L. Ceseracciu, S. Marras, A. Athanassiou, I.S. Bayer, Electrical conductivity enhancement in thermoplastic polyurethane-graphene nanoplatelet composites by stretch-release cycles, Appl. Phys. Lett. 110 (12) (2017) 121904.
[27] V. Eswaraiah, V. Sankaranarayanan, S. Ramaprabhu, Graphene-based engine oil nanofluids for tribological applications, Acs Appl. Mater Inter 3 (11) (2011) 4221–4227.
[28] X.D. Wei, L. Mao, R.A. Soler-Crespo, J.T. Paci, J.X. Huang, S.T. Nguyen, H.D. Espinosa, Plasticity and ductility in graphene oxide through a mechanochemically induced damage tolerance mechanism, Nat. Commun. 6 (2015).
[29] X. Zhao, Q.H. Zhang, D.J. Chen, P. Lu, Enhanced mechanical properties of graphene-based poly(vinyl alcohol) composites, Macromolecules 43 (5) (2010) 2357–2363.
[30] D. Lahiri, R. Dua, C. Zhang, I. de Socarraz-Novoa, A. Bhat, S. Ramaswamy, A. Agarwal, Graphene nanoplatelet-induced strengthening of UltraHigh molecular weight polyethylene and biocompatibility in vitro, Acs Appl. Mater Inter 4 (4) (2012) 2234–2241.
[31] Z. Xu, C. Gao, In situ polymerization approach to graphene-reinforced Nylon-6 composites, Macromolecules 43 (16) (2010) 6716–6723.
[32] P. Cataldi, I.S. Bayer, G. Nanni, A. Athanassiou, F. Bonaccorso, V. Pellegrini, A.E.D. Castillo, F. Ricciardella, S. Artyukhin, M.A. Tronche, Y. Gogotsi, R. Cingolani, Effect of graphene nano-platelet morphology on the elastic modulus of soft and hard biopolymers, Carbon 109 (2016) 331–339.
[33] Y. He, W.F. Chen, W.B. Yu, G. Ouyang, G.W. Yang, Anomalous interface adhesion of graphene membranes, Sci. Rep. 3 (2013).
[34] S.P. Koenig, N.G. Boddeti, M.L. Dunn, J.S. Bunch, Ultrastrong adhesion of graphene membranes, Nat. Nanotechnol. 6 (9) (2011) 543–546.
[35] N. Wei, X.S. Peng, Z.P. Xu, Understanding water permeation in graphene oxide membranes, Acs Appl. Mater Inter 6 (8) (2014) 5877–5883.
[36] W.Z. Zhai, N. Srikanth, L.B. Kong, K. Zhou, Carbon nanomaterials in tribology, Carbon 119 (2017) 150–171.
[37] D. Berman, A. Erdemir, A.V. Sumant, Graphene: a new emerging lubricant, Mater. Today 17 (1) (2014) 31–42.
[38] K.S. Kim, H.J. Lee, C. Lee, S.K. Lee, H. Jang, J.H. Ahn, J.H. Kim, H.J. Lee, Chemical vapor deposition-grown graphene: the thinnest solid lubricant, Acs Nano 5 (6) (2011) 5107–5114.
[39] Y. Huang, Q. Yao, Y. Qi, Y. Cheng, H. Wang, Q. Li, Y. Meng, Wear evolution of monolayer graphene at the macroscale, Carbon 115 (2017) 600–607.
[40] X.Z. Zeng, Y.T. Peng, H.J. Lang, A novel approach to decrease friction of graphene, Carbon 118 (2017) 233–240.
[41] G.N. Ren, Z.Z. Zhang, X.T. Zhu, B. Ge, F. Guo, X.H. Men, W.M. Liu, Influence of functional graphene as filler on the tribological behaviors of Nomex fabric/phenolic composite, Compos Part a-Appl S 49 (2013) 157–164.
[42] D. Lahiri, F. Hec, M. Thiesse, A. Durygind, C. Zhang, A. Agarwal, Nanotribological behavior of graphene nanoplatelet reinforced ultra high molecular weight polyethylene composites, Tribol. Int. 70 (2014) 165–169.
[43] S.S. Kandanur, M.A. Rafiee, F. Yavari, M. Schrameyer, Z.Z. Yu, T.A. Blanchet, N. Koratkar, Suppression of wear in graphene polymer composites, Carbon 50 (9) (2012) 3178–3183.
[44] D. Berman, A. Erdemir, A.V. Sumant, Few layer graphene to reduce wear and friction on sliding steel surfaces, Carbon 54 (2013) 454–459.
[45] P. Poletto, J. Duarte, M.B. Thurmer, V. dos Santos, M. Zeni, Characterization of polyamide 66 membranes prepared by phase inversion using formic acid and hydrochloric acid such as solvents, Mater Res Ibero Am J. 14 (4) (2011) 547–551.
[46] N. Tanaka, T. Fukushima, Melting and recrystallization in modified porous nylon-6 membranes, Thermochim. Acta 396 (1-2) (2003) 79–85.
[47] E.L. Papadopoulou, F. Pignatelli, S. Marras, L. Marini, A. Davis, A. Athanassiou, I.S. Bayer, Nylon 6,6/graphene nanoplatelet composite films obtained from a new solvent, Rsc Adv. 6 (8) (2016) 6823–6831.
[48] P. Cataldi, I.S. Bayer, F. Bonaccorso, V. Pellegrini, A. Athanassiou, R. Cingolani, Foldable conductive cellulose fiber networks modified by graphene nanoplatelet-bio-based composites, Adv. Electron Mater 1 (12) (2015).
[49] G. Radaelli, J.A. Heredia-Guerrero, M.T. Masood, L. Ceseracciu, A. Davis, R. Carzino, M. Prato, I.S. Bayer, A. Athanassiou, Highly effective antiadhesive coatings from pH-modified water-dispersed perfluorinated acrylic copolymers: the case of vulcanizing rubber, Adv. Mater Interfaces 3 (13) (2016).
[50] N.S. Murthy, S.A. Curran, S.M. Aharoni, H. Minor, Premelting Crystalline Relaxations and Phase-Transitions in Nylon-6 and 6,6, Macromolecules 24 (11) (1991) 3215–3220.
[51] B.J. Briscoe, S.K. Sinha, Wear of polymers, P I Mech. Eng. J J Eng. 216 (J6) (2002) 401–413.
[52] B.R. Lawn, Indentation of ceramics with spheres: a century after Hertz, J. Am. Ceram. Soc. 81 (8) (1998) 1977–1994.
[53] A. Dasari, Z.Z. Yu, Y.W. Mai, G.H. Hu, J.L. Varlet, Clay exfoliation and organic modification on wear of nylon 6 nanocomposites processed by different routes, Compos. Sci. Technol. 65 (15–16) (2005) 2314–2328.
[54] J. Ye, H.S. Khare, D.L. Burris, Transfer film evolution and its role in promoting ultra-low wear of a PTFE nanocomposite, Wear 297 (1–2) (2013) 1095–1102.
[55] K.L. Harris, A.A. Pitenis, W.G. Sawyer, B.A. Krick, G.S. Blackman, D.J. Kasprzak, C.P. Junk, PTFE tribology and the role of mechanochemistry in the development of protective surface films, Macromolecules 48 (11) (2015) 3739–3745.
[56] J. Khedkar, I. Negulescu, E.I. Meletis, Sliding wear behavior of PTFE composites, Wear 252 (5–6) (2002) 361–369.
[57] D.H. Xiang, C.J. Gu, A study on the friction and wear behavior of PTFE filled with ultra-fine kaolin particulates, Mater. Lett. 60 (5) (2006) 689–692.
[58] T. Jiang, Y. Zhu, Measuring graphene adhesion using atomic force microscopy with a microsphere tip, Nanoscale 7 (24) (2015) 10760–10766.